

InfMAE: A Foundation Model in Infrared Modality

Fangcen Liu, Chenqiang Gao* , Yaming Zhang, Junjie Guo, Jinhao Wang, Deyu Meng

Abstract—In recent years, the foundation models have swept the computer vision field and facilitated the development of various tasks within different modalities. However, it remains an open question on how to design an infrared foundation model. In this paper, we propose InfMAE, a foundation model in infrared modality. We release an infrared dataset, called Inf30 to address the problem of lacking large-scale data for self-supervised learning in the infrared vision community. Besides, we design an information-aware masking strategy, which is suitable for infrared images. This masking strategy allows for a greater emphasis on the regions with richer information in infrared images during the self-supervised learning process, which is conducive to learning the generalized representation. In addition, we adopt a multi-scale encoder to enhance the performance of the pre-trained encoders in downstream tasks. Finally, based on the fact that infrared images do not have a lot of details and texture information, we design an infrared decoder module, which further improves the performance of downstream tasks. Extensive experiments show that our proposed method InfMAE outperforms other supervised methods and self-supervised learning methods in three downstream tasks. Our code will be made public at <https://github.com/liufangcen/InfMAE>.

Index Terms—Infrared Foundation Model, Infrared Image Segmentation, Infrared Object Detection, Infrared Small Target Detection.

1 INTRODUCTION

Infrared imaging plays a crucial role and finds extensive application in low-light even dark and smoky conditions [1], [2], [3] since they utilize the thermal radiation of objects for imaging, which can effectively alleviate adverse effects caused by challenging environmental conditions. Currently, computer vision tasks in the infrared vision community, such as object detection [4], [5], and semantic segmentation [6], [7], are explored by task-specific designed models. While these models can yield superior performance on individual tasks, they are often challenged by a lack of transferability.

The foundation model refers to a large, general deep learning model that learns extensive knowledge through pre-training on a large-scale dataset and can be adapted to various downstream tasks by fine-tuning or prompting [8], [9], [10]. The Transformer-based model like ViT [11] is one of the representative vision foundation models, which trains on a large-scale of dataset and outperforms the ResNet-based method [12] on the downstream tasks. To better learn the powerful representation of a foundation model from a large number of unlabeled data, self-supervised learning is the primary choice [13]. The self-supervised learning frameworks, such as BEiT [14], DINO [15], and Mask Autoencoders (MAE) [16], achieve impressive performance across various downstream vision tasks [17], [18]. Notably, MAE [16] has verified superior representation learning ability and scalability. This model is pre-trained on the ImageNet-1K dataset [19]. Then, the pre-trained encoder of the MAE [16] serves as a sufficient feature extraction backbone, achiev-

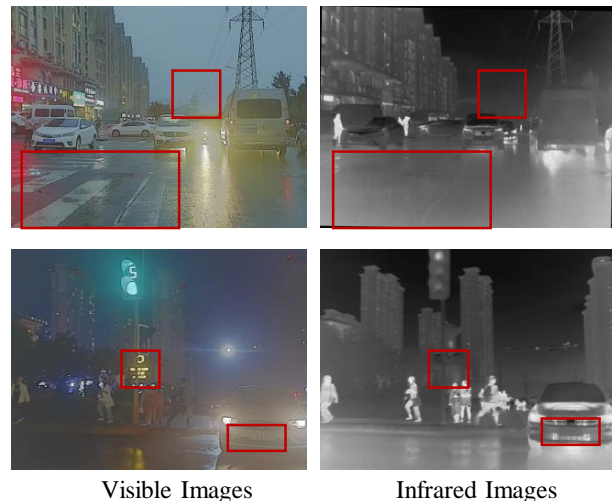


Fig. 1. Visual comparison of infrared and visible images. The infrared image lacks color and texture information, making the information in the whole image not as rich as that in the visible image. For instance, within the red box, objects such as zebra crossings, long-distance telephone poles, road signs, etc., tend to be submerged in the background due to their temperatures being similar.

ing excellent performance on classification, detection, and segmentation tasks. Following the self-supervised learning frameworks, pre-trained foundation models have emerged in various modalities, e.g., VideoMAE [20], [21] in the video modality, Scale-MAE [22] in the remote sensing image modality, and Point-M2AE [23] in the point cloud modality. However, a comparable foundation model has not yet emerged in the infrared modality.

Intuitively, a feasible solution is to directly employ the pre-trained visible MAE on infrared downstream tasks. However, our experimental results (see the details in Section 5.6) show that this is not the optimal solution due to that there are significant differences in imaging char-

*Corresponding author: Chenqiang Gao.

Fangcen Liu, Yaming Zhang, and Junjie Guo are with the School of Communications and Information Engineering, Chongqing University of Posts and Telecommunications, Chongqing 400065, China (E-mail: liufc67@gmail.com, YummyZhang1989@gmail.com, s220101036@stu.cqupt.edu.cn).

Chenqiang Gao and Jinhao Wang are with the School of Intelligent Systems Engineering, Sun Yat-sen University, Shenzhen, Guangdong 518107, China. E-mail: gaochq6@mail.sysu.edu.cn, wangjh298@mail2.sysu.edu.cn.

Deyu Meng is with the School of Mathematics and Statistics, Xi'an Jiaotong University, Xi'an, Shanxi, 710049, China. (E-mail: dymeng@mail.xjtu.edu.cn).

acteristics between infrared and visible modalities. Fig. 1 shows some examples of infrared and visible images. We can observe that infrared images exhibit less information compared to visible images, which lack rich texture, color, and fine details. For instance, objects like zebra crossings and power lines in Fig. 1 lack color and texture information in infrared images, making them indistinguishable from the background. These differences cause a noticeable gap between the infrared and visible modalities. The most direct approach to bridging this gap is to train the MAE model on a large-scale infrared dataset. However, there appears to be a limited availability of a large-scale dataset in the infrared modality. Consequently, it becomes important to build a large-scale infrared dataset to facilitate the training of an infrared foundation model. In this paper, we begin by constructing a large-scale infrared dataset, named Inf30, to address the existing data scarcity within the infrared modality.

Due to the less information on infrared images, directly applying the vanilla MAE [16] architecture to the infrared modality is also a feasible but not the optimal choice, as the experiment shows in Sections 5.2.2, 5.3.2 and 5.4.2. The vanilla MAE adopts the random mask strategy. Directly applying this strategy to infrared images may cause the masking tokens to focus more on the information-poor part which is less conducive to representation learning. Some works [24], [25] argued that masking tokens which have rich semantic information can improve the representation learning ability of the self-supervised method, and introduced the semantic-guided masking strategy. However, these methods do not account for the unique characteristics of the infrared modality and require the addition of new semantic-aware branches in the framework.

In this paper, we propose a first simple yet effective foundation model in the infrared modality named InfMAE that can be extensively generalized to downstream tasks, such as infrared semantic segmentation, object detection, and small target detection. To enhance the representation capabilities for infrared images, we design an information-aware masking strategy, which facilitates the selective masking of regions with richer information without designing an additional semantic awareness branch. In addition, we employ a multi-scale strategy to improve the performance of the pre-trained encoder in downstream tasks. Finally, based on the characteristics of infrared images, we design a new infrared decoder module for image reconstruction. This design further improves the performance of downstream tasks.

We summarize the main contributions of the paper as follows:

- We release an infrared dataset Inf30 for self-supervised learning, which consists of 305241 infrared images.
- We propose the InfMAE, a simple yet effective foundation model in the infrared modality. To the best of our knowledge, this is the first attempt to build a foundation model within the infrared modality.
- Considering the characteristics of infrared imaging, we design an information-aware masking strategy and an infrared decoder. These designs enhance the

model’s ability to learn infrared representations.

- The experimental results show that the method proposed in this paper outperforms state-of-the-art methods, achieving the best performance in downstream tasks.

The remainder of this paper is organized as follows: In Section 2, related works are briefly reviewed. In Section 3, we introduce the details of the Inf30 dataset. In Section 4, we present the proposed method in detail. In Section 5, the experimental results are given and discussed. Conclusions are drawn in Section 6.

2 RELATED WORK

2.1 The Foundation Model

The foundation models are trained on a large-scale dataset in a self-supervised manner, making them adaptable for various downstream tasks [9]. The foundation model can be categorized into four categories based on different inputs: traditional models, textually prompted models, visually prompted models, and heterogeneous modalities-based models [8]. Traditional foundational models usually take only images as input, such as ResNet [26] based on convolutional neural networks, as well as ViT [11] based on the Transformer architecture. The textually prompted models like CLIP [10] and GPT-4 [27] took the textual prompt and the image as the inputs, and the textual prompt established correlations between text and images, contributing to achieving zero-shot transfer. The visually prompted models [28], [29] could be prompted by various prompt types e.g., text, bounding boxes, or a semantical mask to get the target segmentation. The heterogeneous modalities-based models usually combine the various prompt types and the aligned multiple paired modalities e.g., image-audio, image-video, etc., to learn meaningful representations. The ImageBind [30] is the representative work.

In this study, we make the first attempt to explore the foundation model in the infrared modality.

2.2 The Masked Image Modeling and Representation Learning

The Masked Image Modeling (MIM) [14], [16], [31], [32] is an emerging self-supervised learning approach, i.e., by randomly masking a part of the input image and then reconstructing it. This learning method is simple yet effective in learning representations with high generality from a large-scale of data for downstream takes. BEiT [14] and MAE [16] are pioneering works. BEiT [14] used a bidirectional encoder representation to recover the original visual token based on the corrupted image patches. MAE [16] pre-trained the ViT encoder by randomly masking the image tokens, feeding the visible tokens into the encoder, and then reconstructing the masked tokens through the decoder. Based on MAE, pre-trained foundation models based on MIM learning have emerged in various modalities, e.g., VideoMAE [20], [21] in the video modality, Scale-MAE [22] in the remote sensing image modality, and Point-M2AE [23] in the point cloud modality. However, a MIM-based foundation model is not yet available in the infrared modality.

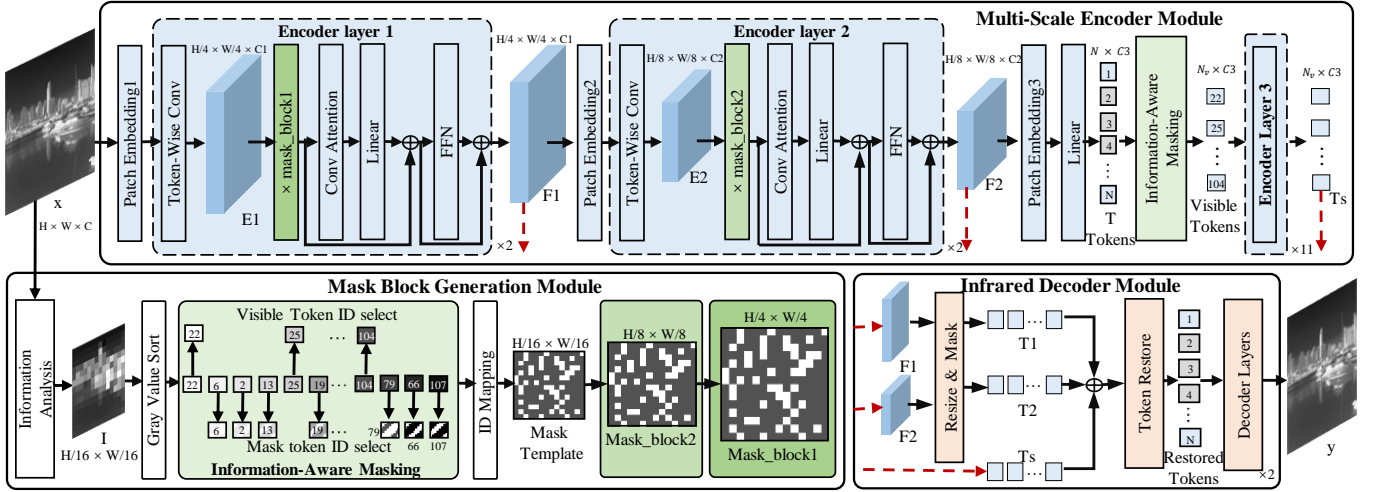


Fig. 2. The framework of the proposed InfMAE. It contains three modules: the mask block generation module, the multi-scale encoder module, and the infrared decoder module. The features connected by the red dashed lines in the multi-scale encoder module are fed into the infrared decoder module.

In addition to extending MIM methods to other modalities, methods also focus on designing mask strategies and how to reconstruct images. Regarding the masking strategy, methods like MST [33] and ATTMask [25] utilized attention maps to guide the masking strategy. SemMAE [24] used semantic information in images to select mask regions. UM-PVT [34] adopted a unified mask approach for masking learning. Regarding image reconstruction, some works [14], [35] adopted tokens produced by VQ-VAE [36] or its variants.

In this study, we explore a new masking strategy and decoder structure for infrared image reconstruction, according to the characteristics of infrared images.

3 PRE-TRAINING DATASET PREPARATION: INF30

3.1 Collection and Preprocessing

A large-scale dataset is essential for training the foundation model. Hence, this study has constructed a dataset named Inf30. The diversity of the images is important for learning the generalized representation. Hence, we extensively collect the infrared image from various websites [37], [38], [39], [40], [41], [42] or capture by ourselves [43]. However, the quality of these images is uneven. For example, the images extracted from the same video exhibit significant similarity, leading to a reduction in image diversity. Additionally, some infrared images obtained from the internet pose challenges due to their extremely low resolution. Consequently, we initiate preprocessing all of the collected images to improve the quality of the infrared dataset.

As for the issue of high similarity in infrared images, we initially selected one image as the anchor. Subsequently, we eliminated those images that have a closely resembling scene with the anchor image and retained images that exhibit substantial dissimilarity. As for the issue of low resolution, we conducted data cleaning by removing images with both width and height of less than 20 pixels.

After collecting and preprocessing the infrared images, we finally obtained 305,241 images. The scene in our dataset

encompasses skies, seascapes, forests, urban areas, suburban areas, lawns, and schools, while the foreground objects include various types of ships, vehicles, pedestrians, public facilities, and residential buildings. The minimum resolution of images is 40×23 , and the maximum resolution of images is 6912×1024 .

3.2 Detail Information Analysis

In this section, we analyze the detail richness of our Inf30 and the well-established ImageNet-1K [19]. We employ the information entropy to measure the information of an image, which can reflect the detail richness. The information entropy is defined as follows:

$$H(X) = - \sum_{i=1}^n P(x_i) \cdot \log_2(P(x_i)), \quad (1)$$

where n is the number of brightness levels in the image, x_i represents each brightness level, and $P(x_i)$ is the probability of the brightness level in the image. We calculate the information entropy of images in the Inf30 and ImageNet-1K datasets. The average information entropy of Inf30 is 6.44, while the average information entropy of ImageNet-1K is 7.19. This reveals that the visible dataset exhibits richer information compared to the infrared image dataset. Recognizing the low information richness of infrared images, this study introduces an information-aware masking strategy to enhance the generalized representation learning ability of the foundation model.

4 METHOD

4.1 Overview

As shown in Fig. 2, the proposed InfMAE consists of three components: 1) the mask block generation module, 2) the multi-scale encoder module, and 3) the infrared decoder module. In the mask block generation module, we adopt an information-aware masking strategy on input tokens to get visible token IDs, mask_block1, and mask_block2, which

are used in the multi-scale encoder module. In the multi-scale encoder module, inspired by MCMAE [31], we combine convolution and self-attention mechanisms to conduct multi-scale feature learning for the visible tokens. In the infrared decoder module, we reshape the multi-scale feature maps obtained by the multi-scale encoder module to the same size and mask them according to the visible token IDs. Then we feed the reshaped multi-scale mask tokens and learned visible tokens into the infrared decoder for image reconstruction.

4.2 The Structure of the Proposed InfMAE

4.2.1 The Mask Block Generation Module

Since infrared images lack color, texture, and fine details, vanilla MAE employs random masks on infrared image input tokens would result in excessive masking of information-poor parts. On the contrary, the proposed information-aware masking strategy can dynamically adjust mask tokens according to the image context.

Given an input image $x \in \mathbb{R}^{H \times W \times C}$, where C , H , and W are input channel, height, and width, respectively. x is first input into the information analysis part to get the intensity-wise feature map. Then we calculate the mean value of the intensity-wise feature map along the channel dimension and obtain the gray value map $I \in \mathbb{R}^{\frac{H}{16} \times \frac{W}{16}}$. After that, the gray value map is flattened to N tokens, $N = \frac{H}{16} \times \frac{W}{16}$. Meanwhile, these tokens are sorted based on the gray value, where a higher-ranking token means that the image information is richer. As depicted in the lower right corner of Fig. 2, each box represents a token, and the number within the box is the token ID. After that, we perform the information-aware masking strategy on the sorted tokens, with a sampling stride S . Specifically, we select the first of every S sorted tokens as a visible token and the rest as masked tokens. Meanwhile, we record the orders of the visible tokens' IDs and the masked tokens' IDs. These IDs will be used as a reference for generating mask blocks.

For mask block generation, we first obtain a binary value mask template through the ID mapping according to the sorted tokens IDs. In the mask template in Fig. 2, the white area is the visible part while the black area is the masked part. Then we up-sample the mask template to get the mask_block2 and mask_block1 for the following multi-scale learning in the multi-scale encoder module.

4.2.2 The Multi-scale Encoder Module

Inspired by previous works like MCMAE [31] and ConvNeXt [44], we introduce a multi-scale encoder for visible token learning. This multi-scale encoder module mainly contains three encoder layers, which are two CNN-based encoders, named encoder layer 1 and encoder layer 2, and one Transormer-based encoder, named encoder layer 3. Such three encoder layers can output feature maps with multi-scale spatial resolution, which are $F_1 \in \mathbb{R}^{\frac{H}{4} \times \frac{W}{4} \times C_1}$, $F_2 \in \mathbb{R}^{\frac{H}{8} \times \frac{W}{8} \times C_2}$, and $T_s \in N_v \times C_3$, respectively. The N_v is the number of the visible tokens. Specifically, we first input the image x into the patch embedding 1 and encoder layer 1 to obtain the feature map F_1 . It should be noted that after the patch embedding 1 and token-wise convolution, we obtain the feature map $E_1 \in \mathbb{R}^{\frac{H}{4} \times \frac{W}{4} \times C_1}$, and then we dot E_1 and

mask_block1 which are obtained in mask block generation module to mask the original feature. Finally, we follow [31] and adopt the convolutional attention (Conv Attention) and FFN. Same as encoder layer 1, the F_1 is inputted into patch embedding 2 and encoder layer 2 to obtain the feature maps $F_2 \in \mathbb{R}^{\frac{H}{8} \times \frac{W}{8} \times C_2}$.

After the patch embedding 3 and a linear operation, the F_2 is patched into N tokens $T \in N \times C_3$. Then, we select the visible tokens from the N tokens according to the visible token IDs obtained by the mask block generation module. Finally, we use the encoder layer 3 whose structure is the same as the ViT [11] encoder layer, and obtain the learned visible tokens $T_s \in N_v \times C_3$.

4.2.3 The Infrared Decoder Module

In this study, we combine the multi-scale visible tokens and mask tokens and take them into the decoder for image reconstruction. Specifically, we normalize the multi-scale features F_1 and F_2 to the same size and then flatten them into the same shape with T . After that, we adopt the same information-aware masking strategy as mentioned in section 4.2.2 to get the visible tokens T_1 and T_2 . Then, we add all the values of visible tokens T_1 , T_2 , and T_s and concat both masked tokens and visible tokens along the first dimension. Meanwhile, we restore the order of these tokens based on the ID number in the mask block generation module. We feed the restored tokens into the decoder for image reconstruction. It is worth noting that infrared images lack many details and color information, so in this study, we adopt a two-layer transformer decoder module for image reconstruction, whose structure is the same as MAE [16].

The loss function measures the Mean Square Error (MSE) between the masked patches of reconstructed image y and the original image x . The MSE loss is defined as follows:

$$\mathcal{L}_{mse} = \frac{1}{M} \sum_{i=1}^M (y_i - x_i)^2, \quad (2)$$

where the M means the number of images.

4.3 InfMAE for Downstream Tasks

After the self-supervised pre-training, InfMAE learns multi-scale feature maps, which can be employed for existing infrared semantic segmentation, object detection, and small target detection methods. To finetune InfMAE for these downstream tasks, we extract the F_1 and F_2 obtained by the encoder layer 1 and encoder layer 2. Meanwhile, we reshape T_s to the feature F_3 and downsample the F_3 to F_4 by a convolution layer. Finally, F_1 , F_2 , F_3 , and F_4 are input into the downstream methods.

5 EXPERIMENT

To validate the proposed InfMAE, we conduct self-supervised pre-training on the proposed Inf30 dataset. Then, the foundation model InfMAE is tested on downstream tasks. Finally, we conduct some ablation studies to explore the validation of the proposed InfMAE.

TABLE 1

Comparison with different semantic segmentation methods on MSRS-inf [45] dataset, where Sup. (Scratch) indicates training our method from scratch. The red and blue marks denote the best and suboptimal results, respectively.

Methods	Backbone	Model	Car(%)	Person(%)	Bike(%)	Curve(%)	Car_Stop(%)	Guardrail(%)	Color_Cone(%)	Bumb(%)	mIoU(%)	mAcc(%)
UperNet [46]	Resnet50	-	82.6	67.2	64.2	47.3	55.1	56.6	53.9	65.9	65.6	74.7
DeeplabV3+ [47]	Resnet50	-	84.2	69.5	63.7	45.1	54.7	68.8	44.5	58.8	65.2	73.8
FPN [48]	Resnet50	-	81.9	66.3	63.4	44.5	55.8	51.1	50.7	54.2	62.9	71.4
ISANet [49]	Resnet50	-	86.1	65.8	68.0	50.1	64.4	69.5	51.2	56.8	67.8	74.9
Sup.(Scratch)	ViT-B	FCN	75.4	63.7	55.9	36.4	49.1	46.9	28.6	55.7	56.5	63.4
Vanilla MAE [16]	ViT-B	FCN	83.2	67.3	62.6	44.5	58.1	57.7	45.0	60.5	64.1	71.6
UM-VPT [34]	VPT-S	FCN	80.3	67.3	61.4	41.1	54.2	59.1	38.7	61.9	62.4	70.1
MCMAE [31]	ViT-B	FCN	86.5	68.8	66.8	55.0	68.3	67.0	52.3	72.7	70.6	78.7
InfMAE(Ours)	ViT-B	FCN	88.2	70.1	68.2	56.1	70.0	67.5	54.5	74.9	72.0	80.0
Sup.(Scratch)	ViT-B	UperNet	74.0	50.7	41.2	49.7	35.6	40.5	44.0	55.9	61.1	61.1
Vanilla MAE [16]	ViT-B	UperNet	86.6	72.3	66.0	56.2	69.7	70.2	54.9	68.1	71.4	78.2
UM-VPT [34]	VPT-S	UperNet	87.2	72.1	66.6	54.0	63.8	56.4	52.1	69.0	68.8	76.3
MCMAE [31]	ViT-B	UperNet	87.5	73.2	66.5	57.1	69.7	67.2	57.0	73.0	72.1	79.8
InfMAE(Ours)	ViT-B	UperNet	89.3	72.8	68.8	59.1	72.1	76.7	57.1	74.2	74.3	82.5

TABLE 2

Performances of different object detection methods on M3FD-inf [50] dataset, where Sup. (Scratch) indicates training our method from scratch. The red and blue marks denote the best and suboptimal results, respectively.

Methods	Backbone	Model	People(%)	Car(%)	Bus(%)	Motor(%)	Lamp(%)	Truck(%)	mAP(%)	AP50(%)
YoloV8 [51]	CSPDarkNet	-	42.8	54.3	58.2	32.5	16.2	40.7	40.8	63.0
FastRCNN [52]	ResNet101	-	39.5	59.6	70.5	37.2	14.4	52.2	25.2	45.6
DINO [15]	Swin-L	-	83.2	87.5	85.6	61.5	60.4	73.5	45.3	75.3
DETR [53]	ResNet101	-	78.5	88.1	87.8	75.8	65.9	78.1	46.7	79.0
Sup.(Scratch)	ViT-B	Mask R-CNN	83.3	88.6	90.1	72.4	66.4	79.1	48.7	80.0
Vanilla MAE [16]	ViT-B	Mask R-CNN	84.8	89.6	93.1	76.0	76.5	80.5	51.4	83.4
MCMAE [31]	ViT-B	Mask R-CNN	87.8	90.8	93.1	87.7	85.9	84.9	55.7	88.4
InfMAE(Ours)	ViT-B	Mask R-CNN	87.9	90.7	94.6	87.1	85.2	83.2	56.2	88.1
Sup.(Scratch)	ViT-B	Cascade R-CNN	83.7	88.6	91.1	68.2	63.9	79.0	50.9	79.1
Vanilla MAE [16]	ViT-B	Cascade R-CNN	85.2	88.9	94.3	72.2	72.6	79.6	52.8	82.1
MCMAE [31]	ViT-B	Cascade R-CNN	85.6	90.4	93.1	76.8	80.9	83.7	54.7	85.1
InfMAE(Ours)	ViT-B	Cascade R-CNN	85.7	90.4	94.9	81.9	81.4	83.4	55.8	86.3

5.1 Pre-training Setup

The framework of the proposed InfMAE is implemented using pytorch 1.12.0 and accelerated by CUDA 11.6 on 4 A100 GPUs. By default, we set the sampling stride s of the information-aware masking strategy to 4. The number of the encoder layer 1, encoder layer 2, and encoder layer 3 are set to 2, 2, and 11, respectively. Meanwhile, the Transformer-based encoder layer 3 with 768 feature dimensions and 12 attention heads. The number of the infrared decoder layers is set to 2 with 512 feature dimensions and 16 attention heads. We use a 400-epoch cosine learning rate schedule with the first 40 epochs warmed up. The AdamW [54] optimizer is used with a base learning rate of 1.5×10^{-4} , a weight decay of 0.05, and a batch size of 256.

5.2 InfMAE on Image Segmentation

5.2.1 Experimental Setup

The MSRS [45] dataset comprises pixel-level annotated images capturing both infrared and visible urban scenes, totaling 1444 pairs. The training set contains 1083 pairs of infrared and visible images and the testing set consists of 361 image pairs. Labeled with eight common driving-related classes. We utilize the infrared images from the MSRS [45] dataset, which we name MARS-inf in the following description, for experimental performance validation. We adopt UperNet [46] and FCN [55], the hierarchical segmentation network headers, to compare the effectiveness of pre-trained InfMAE with other SOTA methods. We use a 24k iteration polynomial learning rate scheme with the first 1500 iterations warmed up. The AdamW [54] optimizer is used, with

an initial learning rate of $10e-4$, weight decay of 0.05, and a batch size of 2.

5.2.2 Results on MSRS-inf

We compare the proposed method with the supervised methods UperNet [46], DeeplabV3+ [47], FPN [48], ISANet [49], and with the self-supervised methods vanilla MAE [16], MCMAE [31], UM-PVT [34]. We present the Intersection over Union (IoU) for each class, the mean Intersection over Union (mIoU) across all classes, and the mean accuracy (mAcc) performance of all classes for all the mentioned methods in Table 1. To evaluate the generalisability of the proposed InfMAE, we use the FCN [55] and Upernet [46] heads for semantic segmentation experiments. The experimental results show that the proposed foundation model outperforms all the SOTA methods.

5.3 InfMAE on Object Detection

5.3.1 Experimental Setup

The M3FD [50] dataset is an infrared and visible target detection and fusion dataset that contains 4200 images. The dataset labels six targets during driving. We use the infrared images from it for experimental performance validation. In the following description, we call this used dataset M3FD-inf. We follow the most common setting to use the detection head in Mask R-CNN and Cascade R-CNN and fine-tune the pre-trained InfMAE model. We follow most of the settings of the benchmark ViT [11]. We report the performance of the target detection model under 25 epoch cosine scheduling with a base learning rate of $10e-4$ and a weight decay of 0.1. The batch size is set to 2.

TABLE 3

Performances of different infrared small target detection methods on IRSTD-1k dataset, where Sup. (Scratch) indicates training our method from scratch. The red and blue marks denote the best and suboptimal results, respectively.

Methods	Backbone	P_d (%)	AUC(%)	F1(%)	IoU(%)
LPNetGA [59]	-	77.1	60.6	50.8	34.1
DNANet [2]	-	89.6	87.8	76.4	61.8
ISTR [4]	ViT-B	85.8	86.1	69.4	53.1
Sup.(Scratch)	ViT-B	86.1	86.1	72.6	57.0
Vanilla MAE [16]	ViT-B	86.8	86.8	72.8	57.2
MCMAE [31]	ViT-B	74.2	90.8	78.4	64.5
UM-VPT [34]	VPT-S	99.6	88.9	73.5	58.1
InfMAE(Ours)	ViT-B	96.6	91.2	79.5	66.0

5.3.2 Results on M3FD-inf

We compare the proposed method with the supervised methods YoloV8 [51], FastRCNN [52], DINO [15], DETR [53], and with the self-supervised methods vanilla MAE [16], MCMAE [31]. We report the AP50 of each class, the AP and AP50 of all classes' performance of all methods, and the experiment results are shown in Table 2. To evaluate the generalisability of the proposed InfMAE, we adopt the Cascade R-CNN [56] and Mask R-CNN [57] heads for object detection. The experimental results show that the proposed foundation model outperforms most of the SOTA methods.

5.4 InfMAE on Small Target Detection

5.4.1 Experimental Setup

The IRSTD-1k [58] is a well-established infrared small target detection dataset that contains 1000 infrared modal images with pixel-level annotations. The images are in the size of 512×512 . We replace the encoder in [4] with the multi-scale encoder module in InfMAE. During the training phase, we adopt the AdamW [54] optimizer with an initial learning rate of 0.001, a weight decay of 0.05, and a batch size of 2.

5.4.2 Results on IRSTD

According to the [4], [60], we report four main performance metrics of infrared small target detection: positive detection P_d , AUC, pixel-level F1 score $F1$, and IoU in the table 3. The experimental results show that the proposed foundation model outperforms all the SOTA methods.

5.5 Ablation Study of InfMAE

5.5.1 Module Ablation

In this section, we validate the effect of the information-aware masking strategy and multi-scale strategy. We adopt UperNet [46] as the segmentation head and Mask R-CNN [57] as the object detection head. The results are shown in Table 4. From Table 4, we can see that combining the proposed information-aware masking strategy and the introduced multi-scale strategies can achieve better performance in downstream tasks.

5.5.2 Decoder Depth

In this section, we analyze the effects of different decoder depths on the experimental performance of downstream tasks. We set the decoder depth to 2, 4, 8, and 12 respectively, and the experimental performance is shown in the table 5.

TABLE 4

Ablation study on the influence of the masking strategy and multi-scale strategy. The IAM means the information-aware masking strategy.

IAM	Multi-scale	Seg_mIoU(%)	Seg_mAcc(%)	Det_AP50(%)	Det_mAP(%)
-	-	71.4	78.2	81.5	49.1
✓	-	72.0	79.4	78.9	50.1
-	✓	72.1	79.8	86.3	55.0
✓	✓	74.3	82.5	88.1	56.2

TABLE 5

The influence of increasing decoder depths on infrared semantic segmentation (UperNet) and object detection (Mask R-CNN).

Decoder Depth	Seg_mIoU(%)	Seg_mAcc(%)	Det_AP50(%)	Det_mAP(%)
2	74.3	82.5	88.1	56.2
4	72.9	80.4	87.9	55.6
8	73.2	80.7	87.6	53.8
12	74.0	81.9	87.2	54.1

From the table, we can see that segmentation and detection gain the best result when the decoder depth is 2. From the experimental results, we can find that the infrared image does not need a deep decoder because of its lack of texture, detail, color, and other information.

5.5.3 Masking Strides

In this section, we analyze the experimental performance under different masking strides. For the mask strides, we select 2, 4, and 7, and the experimental results are shown in the table 6. From the table, we can see that when the masking stride is 4, the semantic segmentation performance is the best, while the AP50 of the detection performance is suboptimal. Since the parameter count of the model increases when the sampling stride is set to 2, we choose a compromise of 4 as the masking strides.

5.5.4 Pre-training Epochs

For MAE, 1600 pre-training epochs can significantly improve the learned representation. We train InfMAE with 200, 400, 800, and 1600 epochs and finetune the pre-trained models on downstream tasks. The experimental results can be seen in Table 7. From this table, we observe improved performances across most downstream tasks with an increase in pre-training epochs.

TABLE 6

The influence of different masking strides of the information-aware masking strategy on infrared semantic segmentation (UperNet) and object detection (Mask R-CNN).

Strides	Seg_mIoU(%)	Seg_mAcc(%)	Det_AP50(%)	Det_mAP(%)
2	74.2	82.0	89.3	56.1
4	74.3	82.5	88.1	56.2
7	71.8	79.9	88.0	54.9

TABLE 7

The influence of increasing pre-training epochs on infrared semantic segmentation (UperNet) and object detection (Mask R-CNN).

Pre-train Epochs	Seg_mIoU(%)	Seg_mAcc(%)	Det_AP50(%)	Det_mAP(%)
200	71.3	78.9	87.4	55.4
400	74.3	82.5	88.1	56.2
800	74.9	83.1	88.3	55.9
1600	74.9	83.2	88.2	56.0

TABLE 8

The influence of different pre-train data scales on infrared semantic segmentation (UperNet) and object detection (Mask R-CNN).

Dataset Scale	Seg_mIoU(%)	Seg_mAcc(%)	Det_AP50(%)	Det_mAP(%)
Inf10	69.1	77.6	86.9	55.0
Inf30	74.3	82.5	88.1	56.2
Inf50	73.0	80.5	87.3	55.8

TABLE 9

The downstream experimental results when using the MAE encoder as the backbone which obtained by different pre-train datasets. When pre-train on infrared images, the downstream tasks can achieve better results in the infrared vision community.

Modality	Pre-train_Data	Seg_mIoU(%)	Det_AP50(%)
RGB	IN1K-30	66.7	78.2
Infrared	Inf30	71.6	83.4

5.5.5 Pre-training Dataset Size Analysis

This subsection reports the performance of downstream tasks when adopting different sizes of pre-training datasets. The results are shown in Table 8. From the table, we can see that the performance gradually increases as the dataset size increases from 100K to 300K. However, when increases from 300K to 500K, the performance is not effectively improved. This can be attributed to the similarity among images in the 500K dataset. In this situation, the representation obtained by the foundation model has limited generalization to the downstream task due to the lack of image diversity. Thus, the quality of the pre-training dataset is significantly important.

5.6 Pre-trained on Inf30 and ImageNet-1K

In this section, we employ the architecture of vanilla MAE [16] to pre-train for 400 epochs on both the infrared Inf30 and IN1K-30 datasets. For fair comparison, the IN1K-30 comprises 300k randomly sampled visible images from ImageNet-1K [19], whose scale is the same as Inf30. Subsequently, we conduct the infrared semantic segmentation on the MASR-inf [45] dataset with UperNet [46] and the infrared object detection on the M3FD-inf [50] dataset with Mask R-CNN [57] to evaluate the generalization capabilities of the pre-trained foundation models. The experiment set is the same MAE [16]. The experimental results are detailed in Table 9. From this table, MAE [16] pre-trains on Inf30 exhibit stronger generalization capabilities in infrared downstream tasks. This observation underscores that the distribution variances indeed contribute to performance disparities. Hence, the release of a large-scale infrared dataset is crucial for the development of the foundation model.

6 CONCLUSION

In this paper, we propose a foundation model in the infrared modality, named InfMAE. We collect a dataset containing 305,241 infrared images for self-supervised learning. Meanwhile, to enhance the model’s capacity to learn the generalized representation, an information-aware masking strategy is proposed, which can make the network pay more attention to the reconstruction of the information-rich part of the image. Besides, based on the characteristics of infrared

images, we design a new decoder structure. Finally, we validate the effectiveness of the proposed method InfMAE in infrared semantic segmentation, object detection, and small target detection tasks. The experimental results show that InfMAE can obtain better experimental results than other supervised and self-supervised methods. In addition, we discuss some parameters in InfMAE. We hope that the proposed foundation model InfMAE can promote the development of the infrared vision community.

REFERENCES

- [1] X. Zhang and Y. Demiris, “Visible and infrared image fusion using deep learning,” *IEEE Transactions on Pattern Analysis and Machine Intelligence*, vol. 45, no. 8, pp. 10535–10554, 2023.
- [2] B. Li, C. Xiao, L. Wang, Y. Wang, Z. Lin, M. Li, W. An, and Y. Guo, “Dense nested attention network for infrared small target detection,” *IEEE Transactions on Image Processing*, vol. 32, pp. 1745–1758, 2022.
- [3] X. Chen, C. Gao, C. Li, Y. Yang, and D. Meng, “Infrared action detection in the dark via cross-stream attention mechanism,” *IEEE Transactions on Multimedia*, vol. 24, pp. 288–300, 2021.
- [4] F. Liu, C. Gao, F. Chen, D. Meng, W. Zuo, and X. Gao, “Infrared small and dim target detection with transformer under complex backgrounds,” *IEEE Transactions on Image Processing*, vol. 32, pp. 5921–5932, 2023.
- [5] F. Lin, S. Ge, K. Bao, C. Yan, and D. Zeng, “Learning shape-biased representations for infrared small target detection,” *IEEE Transactions on Multimedia*, pp. 1–12, 2023.
- [6] Y. Li, H. Liu, Z. Tian, and W. Geng, “Near-infrared vascular image segmentation using improved level set method,” *Infrared Physics & Technology*, vol. 131, p. 104678, 2023.
- [7] Z. Tian, H. Liu, and Q. Li, “Vu-net: A symmetric network-based method for near-infrared blood vessel image segmentation,” in *International Conference on Man-Machine-Environment System Engineering*, pp. 275–280, Springer, 2023.
- [8] M. Awais, M. Naseer, S. Khan, R. M. Anwer, H. Cholakkal, M. Shah, M.-H. Yang, and F. S. Khan, “Foundational models defining a new era in vision: A survey and outlook,” 2023.
- [9] R. Bommasani, D. A. Hudson, E. Adeli, R. Altman, S. Arora, S. von Arx, M. S. Bernstein, J. Bohg, A. Bosselut, E. Brunskill, *et al.*, “On the opportunities and risks of foundation models,” *arXiv preprint arXiv:2108.07258*, 2021.
- [10] A. Radford, J. W. Kim, C. Hallacy, A. Ramesh, G. Goh, S. Agarwal, G. Sastry, A. Askell, P. Mishkin, J. Clark, *et al.*, “Learning transferable visual models from natural language supervision,” in *International conference on machine learning*, pp. 8748–8763, PMLR, 2021.
- [11] A. Dosovitskiy, L. Beyer, A. Kolesnikov, D. Weissenborn, X. Zhai, T. Unterthiner, M. Dehghani, M. Minderer, G. Heigold, S. Gelly, *et al.*, “An image is worth 16x16 words: Transformers for image recognition at scale,” in *International Conference on Learning Representations*, 2020.
- [12] A. Kolesnikov, L. Beyer, X. Zhai, J. Puigcerver, J. Yung, S. Gelly, and N. Houlsby, “Big transfer (bit): General visual representation learning,” in *Computer Vision—ECCV 2020: 16th European Conference, Glasgow, UK, August 23–28, 2020, Proceedings, Part V 16*, pp. 491–507, Springer, 2020.
- [13] Z.-Y. Li, S. Gao, and M.-M. Cheng, “Sere: Exploring feature self-relation for self-supervised transformer,” *IEEE Transactions on Pattern Analysis and Machine Intelligence*, vol. 45, no. 12, pp. 15619–15631, 2023.
- [14] H. Bao, L. Dong, S. Piao, and F. Wei, “Beit: Bert pre-training of image transformers,” in *International Conference on Learning Representations*, 2021.
- [15] M. Caron, H. Touvron, I. Misra, H. Jégou, J. Mairal, P. Bojanowski, and A. Joulin, “Emerging properties in self-supervised vision transformers,” in *Proceedings of the IEEE/CVF international conference on computer vision*, pp. 9650–9660, 2021.
- [16] K. He, X. Chen, S. Xie, Y. Li, P. Dollár, and R. Girshick, “Masked autoencoders are scalable vision learners,” in *Proceedings of the IEEE/CVF conference on computer vision and pattern recognition*, pp. 16000–16009, 2022.

- [17] Y. Li, S. Xie, X. Chen, P. Dollar, K. He, and R. Girshick, "Benchmarking detection transfer learning with vision transformers," *arXiv preprint arXiv:2111.11429*, 2021.
- [18] L. Scheibenreif, M. Mommert, and D. Borth, "Masked vision transformers for hyperspectral image classification," in *Proceedings of the IEEE/CVF Conference on Computer Vision and Pattern Recognition*, pp. 2165–2175, 2023.
- [19] J. Deng, W. Dong, R. Socher, L.-J. Li, K. Li, and L. Fei-Fei, "Imagenet: A large-scale hierarchical image database," in *2009 IEEE conference on computer vision and pattern recognition*, pp. 248–255, Ieee, 2009.
- [20] Z. Tong, Y. Song, J. Wang, and L. Wang, "Videomae: Masked autoencoders are data-efficient learners for self-supervised video pre-training," *Advances in neural information processing systems*, vol. 35, pp. 10078–10093, 2022.
- [21] L. Wang, B. Huang, Z. Zhao, Z. Tong, Y. He, Y. Wang, Y. Wang, and Y. Qiao, "Videomae v2: Scaling video masked autoencoders with dual masking," in *Proceedings of the IEEE/CVF Conference on Computer Vision and Pattern Recognition*, pp. 14549–14560, 2023.
- [22] C. J. Reed, R. Gupta, S. Li, S. Brockman, C. Funk, B. Clipp, K. Keutzer, S. Candido, M. Uyttendaele, and T. Darrell, "Scale-mae: A scale-aware masked autoencoder for multiscale geospatial representation learning," in *Proceedings of the IEEE/CVF International Conference on Computer Vision*, pp. 4088–4099, 2023.
- [23] R. Zhang, Z. Guo, P. Gao, R. Fang, B. Zhao, D. Wang, Y. Qiao, and H. Li, "Point-m2ae: multi-scale masked autoencoders for hierarchical point cloud pre-training," *Advances in neural information processing systems*, vol. 35, pp. 27061–27074, 2022.
- [24] G. Li, H. Zheng, D. Liu, C. Wang, B. Su, and C. Zheng, "Semmae: Semantic-guided masking for learning masked autoencoders," *Advances in Neural Information Processing Systems*, vol. 35, pp. 14290–14302, 2022.
- [25] I. Kakogeorgiou, S. Gidaris, B. Psomas, Y. Avrithis, A. Bursuc, K. Karantzas, and N. Komodakis, "What to hide from your students: Attention-guided masked image modeling," in *European Conference on Computer Vision*, pp. 300–318, Springer, 2022.
- [26] K. He, X. Zhang, S. Ren, and J. Sun, "Deep residual learning for image recognition," in *2016 IEEE Conference on Computer Vision and Pattern Recognition, CVPR 2016, Las Vegas, NV, USA, June 27-30, 2016*, pp. 770–778, IEEE Computer Society, 2016.
- [27] OpenAI, "Gpt-4 technical report," *PREPRINT*, 2023.
- [28] T. Lüddecke and A. S. Ecker, "Image segmentation using text and image prompts," in *IEEE/CVF Conference on Computer Vision and Pattern Recognition, CVPR 2022, New Orleans, LA, USA, June 18-24, 2022*, pp. 7076–7086, IEEE, 2022.
- [29] A. Kirillov, E. Mintun, N. Ravi, H. Mao, C. Rolland, L. Gustafson, T. Xiao, S. Whitehead, A. C. Berg, W. Lo, P. Dollár, and R. B. Girshick, "Segment anything," *CoRR*, vol. abs/2304.02643, 2023.
- [30] R. Girdhar, A. El-Nouby, Z. Liu, M. Singh, K. V. Alwala, A. Joulin, and I. Misra, "Imagebind one embedding space to bind them all," in *IEEE/CVF Conference on Computer Vision and Pattern Recognition, CVPR 2023, Vancouver, BC, Canada, June 17-24, 2023*, pp. 15180–15190, IEEE, 2023.
- [31] P. Gao, T. Ma, H. Li, Z. Lin, J. Dai, and Y. Qiao, "Mcm-ae: Masked convolution meets masked autoencoders," *Advances in Neural Information Processing Systems*, vol. 35, pp. 35632–35644, 2022.
- [32] N. Madan, N.-C. Ristea, R. T. Ionescu, K. Nasrollahi, F. S. Khan, T. B. Moeslund, and M. Shah, "Self-supervised masked convolutional transformer block for anomaly detection," *IEEE Transactions on Pattern Analysis and Machine Intelligence*, vol. 46, no. 1, pp. 525–542, 2024.
- [33] Z. Li, Z. Chen, F. Yang, W. Li, Y. Zhu, C. Zhao, R. Deng, L. Wu, R. Zhao, M. Tang, et al., "Mst: Masked self-supervised transformer for visual representation," *Advances in Neural Information Processing Systems*, vol. 34, pp. 13165–13176, 2021.
- [34] X. Li, W. Wang, L. Yang, and J. Yang, "Uniform masking: Enabling mae pre-training for pyramid-based vision transformers with locality," *arXiv preprint arXiv:2205.10063*, 2022.
- [35] X. Dong, J. Bao, T. Zhang, D. Chen, W. Zhang, L. Yuan, D. Chen, F. Wen, N. Yu, and B. Guo, "Peco: Perceptual codebook for bert pre-training of vision transformers," in *Proceedings of the AAAI Conference on Artificial Intelligence*, vol. 37, pp. 552–560, 2023.
- [36] A. Van Den Oord, O. Vinyals, et al., "Neural discrete representation learning," *Advances in neural information processing systems*, vol. 30, 2017.
- [37] Z. He, Y. Cao, Y. Dong, J. Yang, Y. Cao, and C.-L. Tisse, "Single-image-based nonuniformity correction of uncooled long-wave infrared detectors: A deep-learning approach," *Applied optics*, vol. 57, no. 18, pp. D155–D164, 2018.
- [38] OTCBVS, "Otcvbs benchmark dataset collection." <https://vcip1-okstate.org/pbvs/bench/index.html>.
- [39] P.-L. St-Charles, G.-A. Bilodeau, and R. Bergevin, "Mutual foreground segmentation with multispectral stereo pairs," in *Proceedings of the IEEE International Conference on Computer Vision Workshops*, pp. 375–384, 2017.
- [40] A. S. Lab, "Thermal infrared dataset." <https://projects.asl.ethz.ch/datasets/doku.php?id=ir:iricra2014>.
- [41] Z. Xu, J. Zhuang, Q. Liu, J. Zhou, and S. Peng, "Benchmarking a large-scale fir dataset for on-road pedestrian detection," *Infrared Physics & Technology*, vol. 96, pp. 199–208, 2019.
- [42] T. M. Reporter, "Infrared camera finds 6-year-old lost in deep woods." <https://www.youtube.com/watch?v=FajSFRIkIo>.
- [43] C. Gao, Y. Du, J. Liu, J. Lv, L. Yang, D. Meng, and A. G. Hauptmann, "Infar dataset: Infrared action recognition at different times," *Neurocomputing*, vol. 212, pp. 36–47, 2016.
- [44] S. Woo, S. Debnath, R. Hu, X. Chen, Z. Liu, I. S. Kweon, and S. Xie, "Convnext v2: Co-designing and scaling convnets with masked autoencoders," in *Proceedings of the IEEE/CVF Conference on Computer Vision and Pattern Recognition*, pp. 16133–16142, 2023.
- [45] Linfeng-Tang, "Msrs." <https://github.com/Linfeng-Tang/MSRS>.
- [46] T. Xiao, Y. Liu, B. Zhou, Y. Jiang, and J. Sun, "Unified perceptual parsing for scene understanding," in *Proceedings of the European conference on computer vision (ECCV)*, pp. 418–434, 2018.
- [47] L.-C. Chen, Y. Zhu, G. Papandreou, F. Schroff, and H. Adam, "Encoder-decoder with atrous separable convolution for semantic image segmentation," in *Proceedings of the European conference on computer vision (ECCV)*, pp. 801–818, 2018.
- [48] T.-Y. Lin, P. Dollár, R. Girshick, K. He, B. Hariharan, and S. Belongie, "Feature pyramid networks for object detection," in *Proceedings of the IEEE conference on computer vision and pattern recognition*, pp. 2117–2125, 2017.
- [49] L. Huang, Y. Yuan, J. Guo, C. Zhang, X. Chen, and J. Wang, "Interlaced sparse self-attention for semantic segmentation," *CoRR*, vol. abs/1907.12273, 2019.
- [50] J. Liu, X. Fan, Z. Huang, G. Wu, R. Liu, W. Zhong, and Z. Luo, "Target-aware dual adversarial learning and a multi-scenario multi-modality benchmark to fuse infrared and visible for object detection," in *Proceedings of the IEEE/CVF Conference on Computer Vision and Pattern Recognition*, pp. 5802–5811, 2022.
- [51] ultralytics, "ultralytics." <https://github.com/ultralytics/ultralytics>.
- [52] S. Ren, K. He, R. Girshick, and J. Sun, "Faster r-cnn: Towards real-time object detection with region proposal networks," *Advances in neural information processing systems*, vol. 28, 2015.
- [53] N. Carion, F. Massa, G. Synnaeve, N. Usunier, A. Kirillov, and S. Zagoruyko, "End-to-end object detection with transformers," in *European conference on computer vision*, pp. 213–229, Springer, 2020.
- [54] I. Loshchilov and F. Hutter, "Decoupled weight decay regularization," in *7th International Conference on Learning Representations, ICLR 2019, New Orleans, LA, USA, May 6-9, 2019*, OpenReview.net, 2019.
- [55] J. Long, E. Shelhamer, and T. Darrell, "Fully convolutional networks for semantic segmentation," in *Proceedings of the IEEE conference on computer vision and pattern recognition*, pp. 3431–3440, 2015.
- [56] Z. Cai and N. Vasconcelos, "Cascade r-cnn: Delving into high quality object detection," in *Proceedings of the IEEE conference on computer vision and pattern recognition*, pp. 6154–6162, 2018.
- [57] K. He, G. Gkioxari, P. Dollár, and R. Girshick, "Mask r-cnn," in *Proceedings of the IEEE international conference on computer vision*, pp. 2961–2969, 2017.
- [58] M. Zhang, R. Zhang, Y. Yang, H. Bai, J. Zhang, and J. Guo, "Isnet: Shape matters for infrared small target detection," in *Proceedings of the IEEE/CVF Conference on Computer Vision and Pattern Recognition*, pp. 877–886, 2022.
- [59] F. Chen, C. Gao, F. Liu, Y. Zhao, Y. Zhou, D. Meng, and W. Zuo, "Local patch network with global attention for infrared small target detection," *IEEE Transactions on Aerospace and Electronic Systems*, vol. 58, no. 5, pp. 3979–3991, 2022.
- [60] C. Gao, D. Meng, Y. Yang, Y. Wang, X. Zhou, and A. G. Hauptmann, "Infrared patch-image model for small target detection in a single image," *IEEE transactions on image processing*, vol. 22, no. 12, pp. 4996–5009, 2013.